

Development of ultra-high efficiency soft X-ray angle-resolved photoemission spectroscopy equipped with deep prior-based denoising method

Kohei Yamagami,¹ Yuichi Yokoyama,¹ Yuta Sumiya,² Hayaru Shouno,² Tetsuro Nakamura,¹ and Masaichiro Mizumaki³

¹⁾Japan Synchrotron Radiation Research Institute (JASRI), Sayo, Hyogo 679-5198, Japan.

²⁾The University of Electro-Communications, Department of Informatics, Chofu, Tokyo 182-8585, Japan.

³⁾Faculty of Science, Kumamoto University, Kurokami, Kumamoto 860-8555, Japan.

(*Electronic mail: kohei.yamagami@spring8.or.jp)

(Dated: 1 December 2025)

Soft X-ray angle resolved photoemission spectroscopy (SX-ARPES) is one of the most powerful spectroscopic techniques to visualize the three-dimensional bulk electronic structure in reciprocal lattice space. Compared with ARPES employing low-energy photon sources, the time burden imposed by a lower photoelectron yield, stemming from the photoionization cross-section, has been a persistent technical challenge. To address this challenge, we have developed a noise removal system by using the deep prior-based method and integrated it into the micro focused SX-ARPES (μ SX-ARPES) system at BL25SU in SPring-8. Our implemented system effectively eliminates the grid and spike noise typically present in ARPES data acquired using the voltage Fixed-mode, within about 30 seconds. We demonstrate, through the μ SX-ARPES measurements on a single crystal of CeRu₂Si₂, that data with sufficient statistical accuracy can be obtained in approximately 40 seconds. In addition, we present the potential of high signal-to-noise ratio ARPES measurement, achieving an energy resolution of 51.6 meV at an excitation energy of 708 eV in μ SX-ARPES measurements on polycrystalline gold. Our developed system successfully reduces the time burden in SX-ARPES and paves the way for advancements in lower photoelectron yield measurements, such as those requiring higher energy resolution and three-dimensional nonequilibrium measurements.

I. INTRODUCTION

Angle-resolved photoemission spectroscopy (ARPES) has emerged as a powerful experimental technique for directly visualizing the electronic structure of materials as a function of energy and momentum in reciprocal lattice space¹⁻⁴. Understanding the intricate characteristics of band structures, including topological properties, strongly correlated electron effects, and spin splitting arising from symmetry breaking, is crucial for comprehending the fascinating phenomena observed in condensed matter physics. These phenomena are being progressively explored using vacuum ultraviolet ARPES (VUV-ARPES) with laser and synchrotron light sources⁵⁻⁸. In contrast to VUV-ARPES, soft X-ray ARPES (SX-ARPES) excels in revealing three-dimensional fermiology⁹⁻¹² and probing buried electronic structures, owing to enhancement of bulk sensitivity^{2,13}. This sensitivity stems from the fact that the detection depth in SX-ARPES is empirically observed to be 3-5 times larger than that in VUV-ARPES¹⁴⁻¹⁹. Moreover, the capability of zone-selective band separation through the simultaneous detection of multiple Brillouin zones, facilitated by the wider photoelectron detection angle of advanced photoelectron analyzers^{20,21}, contributes to an accelerated understanding of electronic structures, particularly when employed in conjunction with VUV-ARPES.

However, the photoelectron yield in SX-ARPES remains considerably lower than that in VUV-ARPES in spite of the significant improvements in photon flux and density achieved through the upgraded low-emittance of fourth-generation soft

X-ray synchrotron radiation sources²³⁻²⁸. This fundamental constraint arises primarily from the photoionization cross-section²², which governs the photoemission process. As depicted in Fig. 1(a), the cross-section for valence electrons of typical elements exhibits a strong dependence on photon energy, with the cross-section in the SX region being more than an order of magnitude smaller than that in the VUV region. This reduced cross-section requires longer measurement times in SX-ARPES. Such prolonged acquisition periods risk introducing undesirable effects, such as surface modification or beam drift, which obstruct the accurate determination of the intrinsic electronic structure.

To address the challenge posed by the longer measurement times, the Fixed mode of operation in an electrostatic hemispherical photoelectron analyzer offers a viable solution. In this mode, photoelectrons are measured within a specific kinetic energy-detector angle, limited to the detection area of a two-dimensional detector. This detector typically comprises a multichannel plate (MCP), a phosphor screen, and a camera. Compared to the Swept mode, which involves scanning a wide kinetic energy range, the Fixed mode reduces the acquisition time required to obtain a spectrum with a high signal-to-noise (S/N) ratio. Moreover, this localized measurement mode is particularly well-suited for detailed analysis of the band structure near the Fermi level. However, a common implementation part in an electrostatic hemispherical photoelectron analyzer introduces a potential issue. To block stray photoelectrons, a wire mesh is often placed just before the MCP as a type of electron filter²⁹. Stray photoelectrons are electrons traveling in unintended trajectories enter the detec-

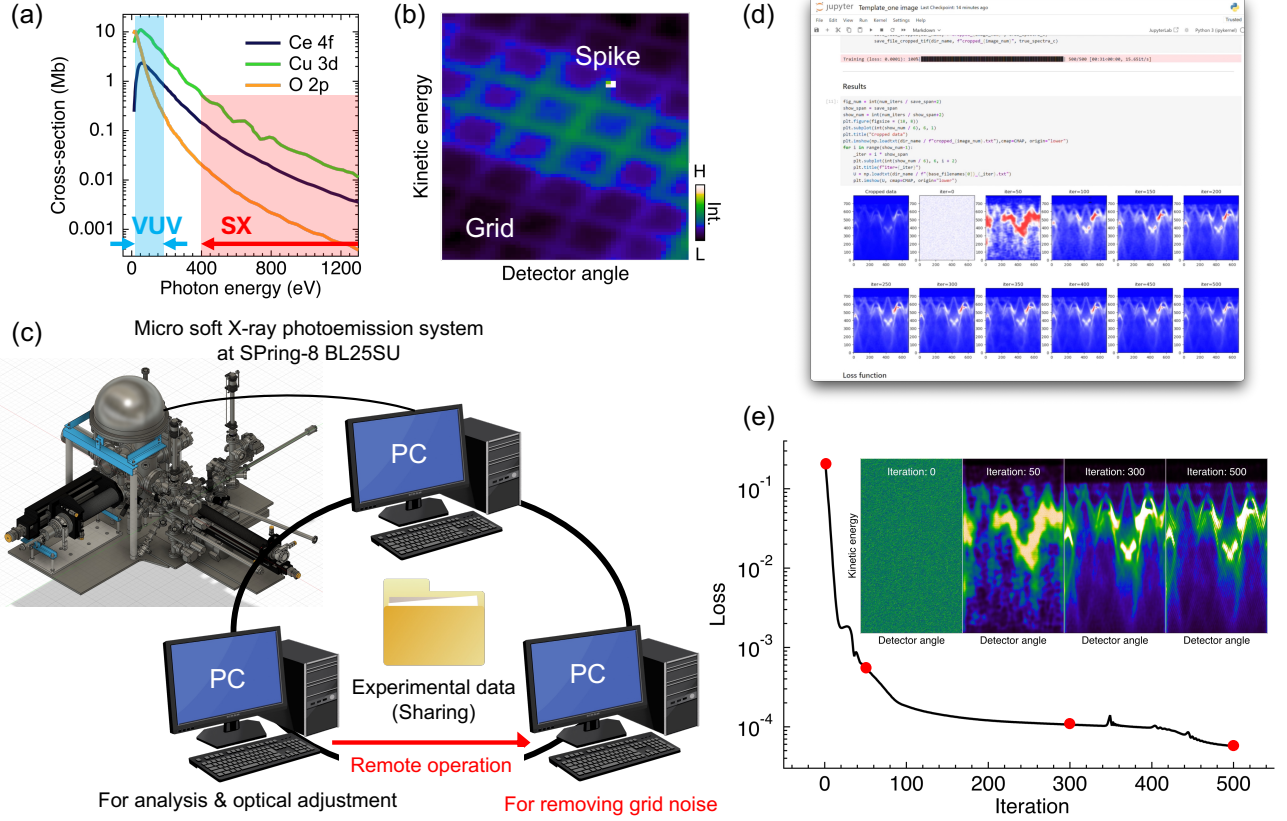


FIG. 1. (a) Photoionization cross-sections of Ce 4*f*, Cu 3*d*, and O 2*p* electrons, digitized from Ref. 22. (b) Grid and spike noise commonly observed in ARPES image obtained by Fixed mode. (c) Overview of the DPDM system implementation. (d) Screenshot of the jupyter Notebook interface after running DPDM. The number of iterations, the degree of completion, and the noise processing time are indicated within the red frame. The ARPES image can be viewed during the denoising process, allowing for real-time monitoring. The optimal denoised data can be selected by referring to the Loss function shown below. (e) Loss function as a function of iterations. The inset ARPES images correspond to the iteration counts indicated by the red circles.

tor during precisely analysis process, which they contribute as background noise to the data, thus lowering the spectrum quality. This mesh leaves traces of a periodic grid structure on the raw data, in addition to the non-periodic spike noise arising from the aging of the detection unit (Fig. 1(b)). Consequently, noise elimination techniques are necessary to remove these artificial artifacts.

Traditional mathematical noise processing methods based on Fourier transforms³⁰ are not ideal for addressing aperiodic spike noise. Moreover, these methods heavily rely on manual adjustments and are sensitive to experimental conditions, potentially compromising the reliability of the processed data. To overcome these limitations, we have recently developed deep prior-based denoising method (DPDM)³¹. This method offers a powerful, training-free approach to image restoration. The technique employs a four-layer U-shaped convolutional neural network with skip connections, leveraging its inherent structural priors alongside an early stopping strategy. This approach effectively separates the intrinsic signal from artifacts and noise, yielding clearer ARPES images in a fraction of the time required by conventional Swept mode.

This paper reports the development of an ultra-high effi-

cient SX-ARPES system capable of acquiring S/N ARPES images and performing denoising within one minute. This system integrates a micro-focusing soft X-ray photoelectron spectroscopy system (μ SX-ARPES) operating at BL25SU of SPring-8 with a newly developed DPDM. Single crystals of CeRu₂Si₂ and Mn₃Si₂Te₆, known for exhibiting clear and indistinct band dispersions, respectively, were selected as test samples to evaluate the accumulation time dependence and capture buried band structure from the background facilitated by the DPDM. Our developed system demonstrates that the DPDM accelerates the high-throughput capabilities of synchrotron-based SX-ARPES and opens up new possibilities for developing low-yield SX-ARPES measurement techniques.

II. OVERVIEW OF THE DENOISE SYSTEM AND ITS IMPLEMENTATION IN THE μ SX-ARPES SYSTEM AT SPRING-8 BL25SU

The μ SX-ARPES system operates at the circularly polarized soft X-ray beamline BL25SU of SPring-8^{32,33}. The avail-

able $h\nu$ range is from 120 eV to 2000 eV. The resolving powers ($h\nu/\Delta h\nu$) of the monochromator typically used range from 10000 for standard ARPES to 20000 for higher energy resolution ARPES. Using the Wolter mirror, a micro beam spot size is typically achieved on the sample^{33,34}. ARPES data are recorded by the DA30 hemispheric analyzer (Scienta Omicron Inc.). This analyzer can perform two-dimensional angular (θ_x - θ_y) mapping while maintaining a fixed geometry between the X-ray source, sample, and DA30, by using a deflector scan perpendicular to the detector slit.

Since BL25SU is a public beamline, in-situ processing must be highly practical to facilitate user access to the DPDM. Therefore, we have developed an environment that enables (i) fast processing, (ii) ease of operation, and (iii) a high degree of flexibility. Figure 1(c) provides an overview of the ultra-high efficiency μ SX-ARPES system environment. In addition to the PC for measurement and analysis/optics, a dedicated PC for DPDM is utilized, and experimental data are shared through a local network connection. The DPDM-PC is operated remotely from the analysis/optics PC. The DPDM-PC is equipped with memory (DDR5 4800MHz RDIMM 16GB \times 8), an SSD (ADD-SSD-S3840G), and a GPU (ADD-NV-RTXA6000) to maximize noise processing and image storage capacity.

The DPDM is operated using Python code implemented in a Jupyter Notebook environment as shown in Figure 1(d). To enhance user-friendliness, the system requires only the input of two-dimensional numerical data and the denoising range to users. The system saves an image of the ongoing process every 10–50 iterations, up to a maximum iteration number. The movie in the Supplementary Information demonstrates the noise processing, which is completed in approximately 30 seconds. After execution, the user selects an appropriate ARPES image by referring to the ARPES image and loss function displayed in the Jupyter Notebook environment. Figure 1(e) presents the ARPES image corresponding to a specific number of iterations and the loss function³¹. Noise reduction is achieved by extracting the band structure from the input image, starting with uniformly distributed random noise. The grid structure is effectively removed at approximately 300 iterations when the loss function reaches a constant value. Beyond 400 iterations, the loss function decreases, reflecting overfitting, and the grid structure gradually re-emerges. Therefore, an ARPES image output between 300 and 400 iterations can be selected as the denoised data.

III. EVALUATION OF EFFICIENCY FOR μ SX-ARPES WITH DENOISE SYSTEM

A. Reducing Accumulation Time

To evaluate the effectiveness of the DPDM in removing grid and spike noise, we first performed μ SX-ARPES measurements on CeRu_2Si_2 as a demonstration. CeRu_2Si_2 is a well-known $4f$ heavy fermion system. The three-dimensional band structure and its spectral analysis using energy distribution curves (EDCs) have been reported in previous SX-ARPES

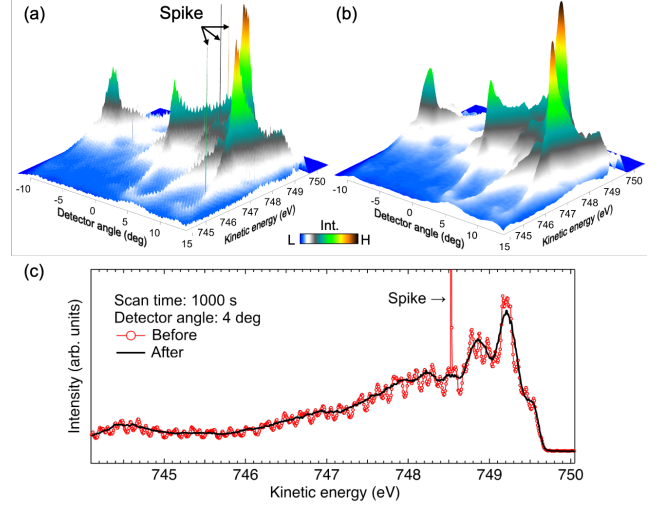


FIG. 2. The upper two figures present 3D surface plots of CeRu_2Si_2 (a) before and (b) after denoising. The data were acquired at $h\nu = 750$ eV and 77 K in Fixed mode with an accumulation time of 1000 seconds, which ensures a sufficient S/N ratio. (c) Comparison of EDC spectra at a detector angle of 4 degrees, before and after denoising, highlighting the removal of grid and spike noise.

studies^{11,35,36}. All subsequent ARPES data were recorded in Fixed mode at $h\nu = 750$ eV with $h\nu/\Delta h\nu = 10000$ and a temperature of 77 K. Figures 2(a) and (b) present the 3D surface plots before and after denoising. The accumulation time was set to 1000 seconds to ensure a sufficient S/N ratio. Despite the presence of significant spike noise in the raw data, alongside the band dispersion, this noise is effectively removed in the processed data. The periodic noise originating from the grid structure is smoothly eliminated from the EDC spectra (Fig. 2(c)). Therefore, we conclude that the DPDM effectively removes grid and spike noise, enabling spectral analysis.

Next, we investigated the potential of the DPDM to reduce the accumulation time. Figures 3(a-d) show the accumulation time dependence of raw kinetic energy-detector angle (E_k - θ) images acquired in Fixed mode. While the data acquired with an accumulation time of 5 seconds exhibit a low S/N ratio due to statistical errors, those acquired with accumulation times longer than 40 seconds appear as smooth images. However, after denoising (Figs. 3(e-h)), the band dispersion can be discerned even in the data acquired with a 5-second accumulation time. Fourier analysis indicates that high-frequency noise originating from the grid structure was effectively removed from both the 10-second and 40-second data³¹. In comparison to the E_k - θ image acquired in Swept mode (Fig. 3(i)) with a 45-minute accumulation time, we conclude that sufficient S/N ratio data can be obtained with an accumulation time of at least 40 seconds. Using Fig. 3(j) and (k), we conducted a more detailed examination of the minimum accumulation time required to achieve an S/N ratio suitable for EDC spectral analysis. The EDC spectrum obtained in Swept mode reveals that the broad structure observed around $E_k = 747.75$ eV comprises two peaks. Using this low-intensity two-peak structure as a benchmark, we determined that the threshold accumula-

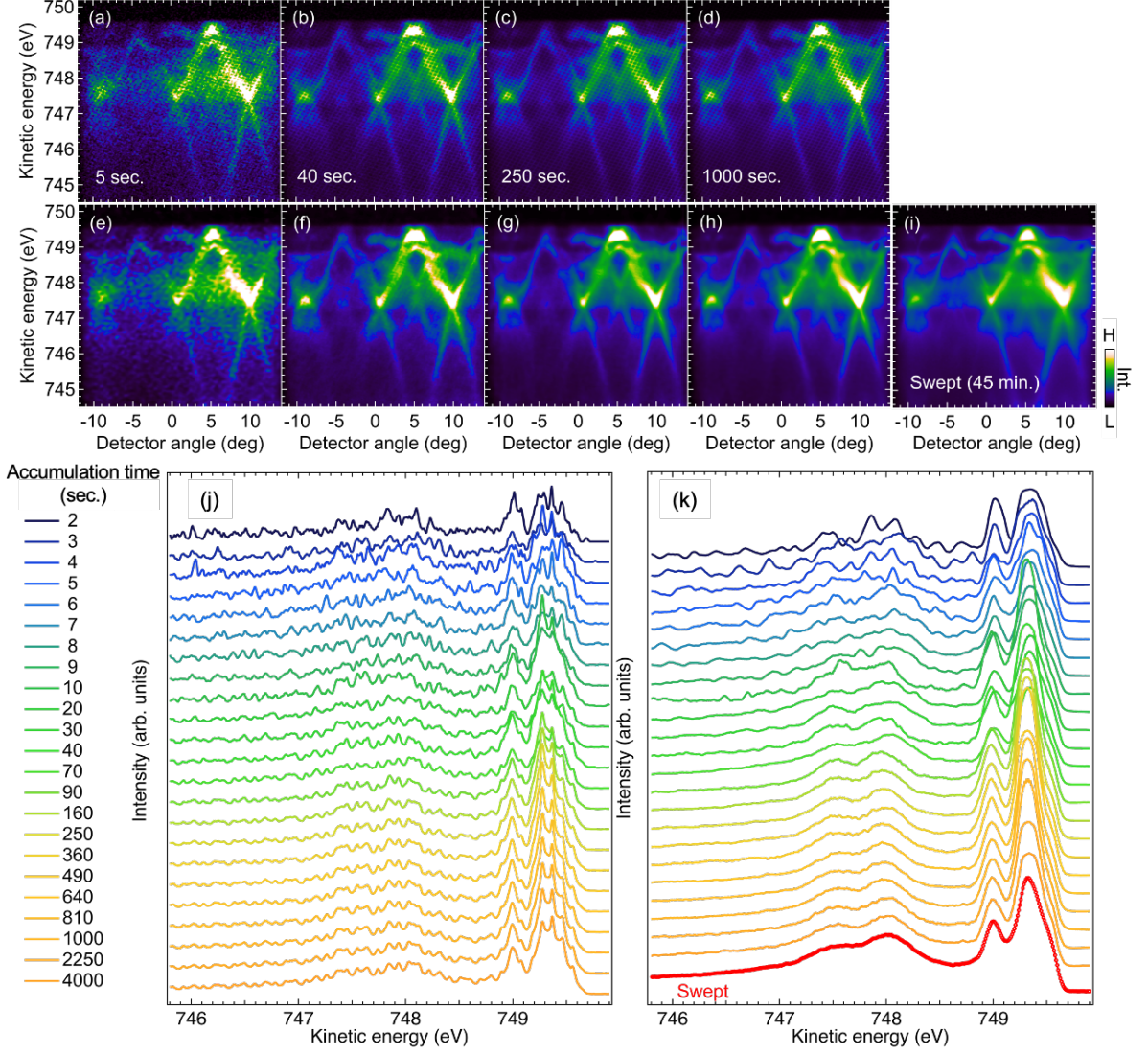


FIG. 3. Relationship between accumulation time and raw kinetic energy-detector angle (E_k - θ) images for CeRu₂Si₂ acquired in Fixed mode. (a-d) E_k - θ images with different accumulation time. (e-h) The same E_k - θ images as panels (a-d), but after denoising. (i) Raw E_k - θ image measured in Swept mode for comparison, with an accumulation time of 45 minutes. (j-k) Comparison of the accumulation time dependent EDC spectra (j) before and (k) after denoising. The EDC spectrum acquired in Swept mode is also shown for comparison.

tion time required for reliable observation of these features in the denoised Fixed mode data is 40 seconds. Therefore, we conclude that statistically reliable SX-ARPES data suitable for spectral analysis can be acquired in approximately one minute, by combining 30 seconds of noise processing with 40 seconds of ARPES data accumulation.

B. Applying To The Material With Indistinct Band Structure

Even when ARPES measurements are performed on an atomically flat and clean surface, the resulting image is not always clear. For example, the scattering of photoelectrons caused by crystal defects, such as impurity atoms, lattice

imperfections, and dislocations, as well as electron-electron interactions, can obscure the band structure. Furthermore, the uncertainty in the perpendicular momentum of photoelectrons, known as k_z -broadening, which is inversely proportional to the detection depth, contributes to the formation of intrinsic background noise^{3,37,38}. To address these challenges, we demonstrate the effectiveness of the DPDM in extracting band structures obscured by crystallographic and fundamental photoemission process effects. We employed a ferrimagnetic semiconductor Mn₃Si₂Te₆ as a test material^{39–41}. Previous VUV-ARPES measurements have shown that the band dispersion is obscured by a significant background⁴². SX-ARPES data were acquired at $h\nu = 500$ eV with $h\nu/\Delta h\nu = 10000$ and below 30 K along Γ - M line within the Brillouin Zone.

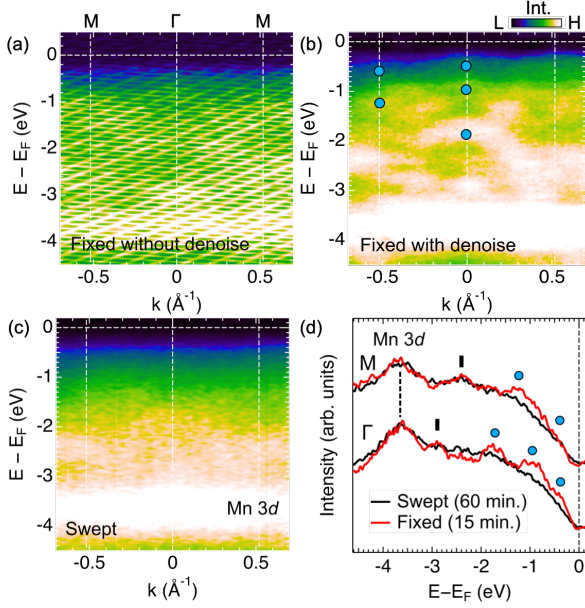


FIG. 4. The binding energy - momentum (E - k) images of $\text{Mn}_3\text{Si}_2\text{Te}_6$ acquired in Fixed mode (a) without and (b) with denoising. (c) The same E - k image, but obtained in Swept mode for comparison. The data were acquired at $h\nu = 500$ eV and a temperature below 30 K along the Γ - M line. (d) EDC spectra at the Γ and M points. The filled circles indicate the peak clearly observed in Fixed mode, but not in Swept mode.

The accumulation time was set to 1000 seconds for Fixed mode and 3600 seconds for Swept mode. Figures 4(a) and (b) present the binding energy - momentum (E - k) image obtained in Fixed mode without and with denoising, respectively. The grid is removed, and multiple band structures are extracted, resulting in sharper image contrast. As shown in Fig. 4(c) for comparison in Swept mode, in addition to a Mn 3d flat band at $E - E_F = -3.6$ eV and a convex band dispersion around $E - E_F = -2.5$ eV, the band dispersion around $E - E_F = -1.0$ eV is more clearly resolved in Fixed mode with denoising. This image sharpening corresponds to the enhanced peak definition in the EDC spectrum (Fig. 4(d)). Compared to VUV-excited photoelectrons, SX-excited photoelectrons have larger escape depth and kinetic energy, which reduces the background associated with projection in the k_z direction and the scattering. However, the broadened EDC spectrum in Swept mode indicates that the background from the voltage sweep and averaged grid structure hinders peak formation. Therefore, we conclude that the DPDM, in conjunction with the advantages of the Fixed mode, effectively eliminates the grid structure to reveal the intrinsic EDC spectra.

TABLE I. List of the detectable photoelectron kinetic energy range (unit: eV) selected by operating mode and E_p in the case of DA30 analyzer at BL25SU in SPring-8.

E_p (eV)	DA30-01 mode	DA14-08 mode
100	12-800	22-1071
75	9-600	18-1167
50	6-400	13-1131

IV. DISCUSSIONS: FUTURE APPLICATIONS AND DEVELOPMENTS

The aforementioned demonstration confirms that the DPDM successfully reduces the accumulation time required to obtain high S/N spectra, without compromising the performance of the μSX -ARPES system. This presents a valuable opportunity to further develop the capabilities of μSX -ARPES and establish new measurement techniques.

The first opportunity lies in the enhancement of the overall experimental energy resolution ΔE_T . Energy resolution has been achieved a continued trend of exponential improvement reported in representative SX-ARPES studies³. ΔE_T value is basically determined by the combined resolutions of the photon source ($\Delta h\nu$) and the photoelectron analyzer (ΔE_A): $(\Delta E_T)^2 = (\Delta h\nu)^2 + (\Delta E_A)^2$. Here $\Delta E_A \approx \frac{w}{2R} E_p$, and w , R , E_p represent the entrance slit width, hemispherical radius, and pass energy, respectively^{43,44}. For the DA30 analyzer at BL25SU of SPring-8, the standard set values are DA30-01 lens operating mode with $w = 0.2$ mm, $R = 200$ mm, and $E_p = 100$ eV, corresponding to $\Delta E_A = 50$ meV. However, with decreasing E_p to 50 eV, the detectable kinetic energies of photoelectron become narrower to 400 eV. In contrast, as shown in Table I about the list of operating mode for DA30, DA14-08 lens mode with a narrower detector angle of $\theta_x = \pm 7$ degrees can measure θ_x - θ_y mapping ($\theta_y = \pm 7$ degrees) for kinetic energies up to 1131 eV even at $E_p = 50$ eV. Actually we measured ARPES on polycrystalline gold in DA14-08 lens mode by Swept mode. The condition was set to $h\nu = 708$ eV with $h\nu/\Delta h\nu = 20000$, $w = 0.3$ mm, $E_p = 50$ eV, corresponding to $\Delta E_T = 51.6$ meV as theoretical value. As shown in Fig. 5, we confirmed that ΔE_T at 30 K is achieved 51.6 meV fitted by Fermi-Dirac distribution to the angle-integrated experimental data with an accumulation time of 2 hours. This energy resolution is improving following an exponential trend of previous SX-ARPES studies³. Therefore, measurements in Fixed mode can achieve faster accumulation times, providing the potential for practical ultra-high-resolution measurements in the soft X-ray region thank to DPDM. Fourth-generation synchrotron radiation facilities have achieved lower emittance, which is expected to lead to higher resolution ($h\nu/\Delta h\nu \geq 30000$) and

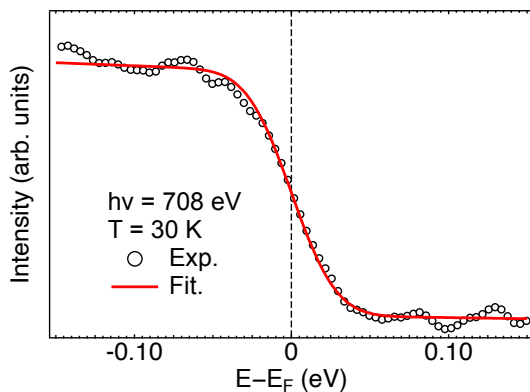


FIG. 5. Angle-integrated ARPES spectrum near the Fermi level of gold in Swept mode. The red solid line represents the fit of the Fermi-Dirac distribution, with a total energy resolution of 51.6 meV, to the data.

brilliance of the photon source^{23–28,45}. For example, when $h\nu/\Delta h\nu = 50000$, $w = 0.2$ mm, and $E_p = 50$ eV in DA30 analyzer, ΔE_T is expected to 29.7 meV at $h\nu = 800$ eV, which can become comparable to that of VUV-ARPES. This would enable the investigation of three-dimensional momentum-resolved fine electronic structures with bulk sensitivity such as High- T_c superconducting cuprates^{1,46–48}.

The second opportunity is the development of coherent synchrotron radiation SX-ARPES for the observation of three-dimensional nonequilibrium electron structures. SPring-8-II plans to achieve an emittance reduction of more than one order of magnitude compared to SPring-8, in the short wavelength region above hard X-ray²⁷. This suggests the possibility of utilizing fully coherent synchrotron radiation in the soft X-ray region. The use of temporal coherence offers significant value to the nonequilibrium studies, as reported by the advancements in time-resolved soft X-ray measurements^{49–57}. Time-resolved ARPES has been pioneered using ultraviolet and extreme ultraviolet laser-based sources^{6,8,58–62}, and soft X-ray sources are crucial for extending these studies to bulk electronic structures in a wider momentum space. The developed DPDM, in conjunction with next-generation synchrotron soft X-ray light sources, is expected to dramatically advance ARPES technology.

V. SUMMARY

We have established an ultra-efficient SX-ARPES measurement environment by integrating deep-prior based denoise system into the μ SX-ARPES system at BL25SU in SPring-8. The challenge posed by the limited photoionization cross-section was overcome by reducing both the denoising processing time and the accumulation time in Fixed mode on the photoelectron analyzer. This also enables the visualization of band dispersion obscured by crystallographic electron scattering and electron correlation. We anticipate that next-generation synchrotron radiation sources and advancements

in the electrical control of photoelectron analyzers will lead to the development of enhanced ARPES technology, facilitating further improvements in energy resolution and enabling the exploration of three-dimensional nonequilibrium electronic structures. Furthermore, the DPDM's capability is not limited to SX-ARPES; it can be readily applied to VUV-ARPES images exhibiting grid structures. The technique is broadly anticipated to be highly effective for a diverse range of experimental image data, spanning applications from periodic background removal in data to the analysis of reflective images in X-ray diffraction, photoelectron diffraction patterns in photoelectron holography, and speckle patterns in X-ray photon correlation spectroscopy.

SUPPLEMENTARY MATERIAL

See the supplementary material for the movie about the denoising program and the Python code and manual of the DPDM system, along with demonstration μ SX-ARPES data for CeRu₂Si₂ accumulated over 1000 seconds.

ACKNOWLEDGMENTS

We thank for T. Ohkochi and Y. Amakai for providing the single crystal sample. The soft X-ray ARPES experiments were performed at the BL25SU of SPring-8 with the approval of the Japan Synchrotron Radiation Research Institute (JASRI) (Proposal No.2023A1354, 2023B2426, 2024A2397, 2024B2440, 2025A2384). This work was supported by Grant-in-Aid for Early-Career Scientists (Grant No.25K17944) and JST PRESTO (Grant No. JPMJPR25JA).

- ¹A. Damascelli, Z. Hussain, and Z.-X. Shen, "Angle-resolved photoemission studies of the cuprate superconductors," *Reviews of Modern Physics* **75**, 473 (2003).
- ²V. N. Strocov, L. Lev, M. Kobayashi, C. Cancellieri, M.-A. Husanu, A. Chikina, N. Schröter, X. Wang, J. A. Krieger, and Z. Salman, "k-resolved electronic structure of buried heterostructure and impurity systems by soft-X-ray ARPES," *Journal of Electron Spectroscopy and Related Phenomena* **236**, 1–8 (2019).
- ³J. A. Sobota, Y. He, and Z.-X. Shen, "Angle-resolved photoemission studies of quantum materials," *Reviews of Modern Physics* **93**, 025006 (2021).
- ⁴H. Zhang, T. Pincelli, C. Jozwiak, T. Kondo, R. Ernstorfer, T. Sato, and S. Zhou, "Angle-resolved photoemission spectroscopy," *Nature Reviews Methods Primers* **2**, 54 (2022).
- ⁵H. Yang, A. Liang, C. Chen, C. Zhang, N. B. Schroeter, and Y. Chen, "Visualizing electronic structures of quantum materials by angle-resolved photoemission spectroscopy," *Nature Reviews Materials* **3**, 341–353 (2018).
- ⁶X. Zhou, S. He, G. Liu, L. Zhao, L. Yu, and W. Zhang, "New developments in laser-based photoemission spectroscopy and its scientific applications: a key issues review," *Reports on Progress in Physics* **81**, 062101 (2018).
- ⁷Y. Li, Q. Wan, and N. Xu, "Recent Advances in Moiré Superlattice Systems by Angle-Resolved Photoemission Spectroscopy," *Advanced Materials*, 2305175 (2023).
- ⁸F. Boschini, M. Zonno, and A. Damascelli, "Time-resolved ARPES studies of quantum materials," *Reviews of Modern Physics* **96**, 015003 (2024).
- ⁹A. Sekiyama, T. Iwasaki, K. Matsuda, Y. Saitoh, Y. Onuki, and S. Suga, "Probing bulk states of correlated electron systems by high-resolution resonance photoemission," *Nature* **403**, 396–398 (2000).
- ¹⁰M. Yano, A. Sekiyama, H. Fujiwara, T. Saita, S. Imada, T. Muro, Y. Onuki, and S. Suga, "Three-Dimensional Bulk Fermiology of CeRu₂Ge₂ in the

- Paramagnetic Phase by Soft X-Ray $h\nu$ -Dependent (700–860 eV) ARPES,” *Physical Review Letters* **98**, 036405 (2007).
- ¹¹M. Yano, A. Sekiyama, H. Fujiwara, Y. Amano, S. Imada, T. Muro, M. Yabashi, K. Tamasaku, A. Higashiya, T. Ishikawa, *et al.*, “Electronic structure of CeRu_2X_2 ($\text{X} = \text{Si, Ge}$) in the paramagnetic phase studied by soft x-ray ARPES and hard x-ray photoelectron spectroscopy,” *Physical Review B* **77**, 035118 (2008).
 - ¹²Y. Nakatani, H. Aratani, H. Fujiwara, T. Mori, A. Tsuruta, S. Tachibana, T. Yamaguchi, T. Kiss, A. Yamasaki, A. Yasui, *et al.*, “Evidence for momentum-dependent heavy-fermionic electronic structures: Soft x-ray ARPES for the superconductor CeNi_2Ge_2 in the normal state,” *Physical Review B* **97**, 115160 (2018).
 - ¹³G. Berner, M. Sing, F. Pfaff, E. Benckiser, M. Wu, G. Christiani, G. Logvenov, H.-U. Habermeyer, M. Kobayashi, V. Strocov, *et al.*, “Dimensionality-tuned electronic structure of nickelate superlattices explored by soft-x-ray angle-resolved photoelectron spectroscopy,” *Physical Review B* **92**, 125130 (2015).
 - ¹⁴M. P. Seah and W. Dench, “Quantitative electron spectroscopy of surfaces: A standard data base for electron inelastic mean free paths in solids,” *Surface and Interface Analysis* **1**, 2–11 (1979).
 - ¹⁵S. Tanuma, C. J. Powell, and D. R. Penn, “Calculations of electron inelastic mean free paths for 31 materials,” *Surface and Interface Analysis* **11**, 577–589 (1988).
 - ¹⁶S. Tanuma, C. J. Powell, and D. R. Penn, “Calculations of electron inelastic mean free paths. II. Data for 27 elements over the 50–2000 eV range,” *Surface and Interface Analysis* **17**, 911–926 (1991).
 - ¹⁷S. Tanuma, C. J. Powell, and D. R. Penn, “Calculations of electron inelastic mean free paths (IMFPs). IV. Evaluation of calculated IMFPs and of the predictive IMFP formula TPP-2 for electron energies between 50 and 2000 eV,” *Surface and Interface Analysis* **20**, 77–89 (1993).
 - ¹⁸S. Tanuma, C. J. Powell, and D. R. Penn, “Calculations of electron inelastic mean free paths (IMFPs) VI. Analysis of the Gries inelastic scattering model and predictive IMFP equation,” *Surface and Interface Analysis* **25**, 25–35 (1997).
 - ¹⁹C. J. Powell and A. Jablonski, “Evaluation of electron inelastic mean free paths for selected elements and compounds,” *Surface and Interface Analysis* **29**, 108–114 (2000).
 - ²⁰H. Fujiwara, Y. Nakatani, H. Aratani, Y. Kanai-Nakata, K. Yamagami, S. Hamamoto, T. Kiss, A. Yamasaki, A. Higashiya, S. Imada, *et al.*, “Impact of the ground-state $4f$ symmetry for anisotropic cf hybridization in the heavy-fermion superconductor CeNi_2Ge_2 ,” *Physical Review B* **108**, 165121 (2023).
 - ²¹Y. Morita, K. Nakanishi, T. Iwata, K. Ohwada, Y. Nishioka, T. Kousa, M. Nurmamat, K. Yamagami, A. Kimura, T. Yamada, *et al.*, “Zone-selection effect of photoelectron intensity distributions in the nonsymmorphic system RAISi ($R = \text{Ce or Nd}$),” *Physical Review B* **111**, L081116 (2025).
 - ²²J. Yeh and I. Lindau, “Atomic subshell photoionization cross sections and asymmetry parameters: $1 \leq Z \leq 103$,” *Atomic Data and Nuclear Data Tables* **32**, 1–155 (1985).
 - ²³P. F. Tavares, E. Al-Dmour, Å. Andersson, F. Cullinan, B. N. Jensen, D. Olsson, D. K. Olsson, M. Sjöström, H. Tarawneh, S. Thorin, *et al.*, “Commissioning and first-year operational results of the MAX IV 3 GeV ring,” *Synchrotron Radiation* **25**, 1291–1316 (2018).
 - ²⁴T. E. Fornek, “Advanced photon source upgrade project final design report,” Tech. Rep. (Argonne National Lab.(ANL), Argonne, IL (United States), 2019).
 - ²⁵P. Raimondi, N. Carmignani, L. Carver, J. Chavanne, L. Farvacque, G. Le Bec, D. Martin, S. Liuzzo, T. Perron, and S. White, “Commissioning of the hybrid multibend achromat lattice at the European Synchrotron Radiation Facility,” *Physical Review Accelerators and Beams* **24**, 110701 (2021).
 - ²⁶P. Klysubun, P. Sudmuang, T. Pulampong, T. Chanwattana, S. Jummunt, P. Sunwong, S. Prawanta, A. Kwankasem, N. Juntong, T. Phimsen, *et al.*, “SPS-II: A 4th generation synchrotron light source in Southeast Asia,” *Proceedings of the 13th International Particle Accelerator Conference, Bangkok, Thailand*, 12–17 (2022).
 - ²⁷T. Watanabe and H. Tanaka, “SPRING-8 upgrade project: accelerator re-designed and restarted,” *Synchrotron Radiation News* **36**, 3–6 (2023).
 - ²⁸S. Obara, K. Ueshima, T. Asaka, Y. Hosaka, K. Kan, N. Nishimori, T. Aoki, H. Asano, K. Haga, Y. Iba, *et al.*, “Commissioning of a compact multibend achromat lattice NanoTerasu: A new 3 GeV synchrotron radiation facility,” *Physical Review Accelerators and Beams* **28**, 020701 (2025).
 - ²⁹J. Liu, D. Huang, Y.-f. Yang, and T. Qian, “Removing grid structure in angle-resolved photoemission spectra via deep learning method,” *Physical Review B* **107**, 165106 (2023).
 - ³⁰S. Liu, E. Kotta, Y. Xu, J. Mutch, J.-H. Chu, M. Hoesch, S. K. Mahatha, J. D. Denlinger, and L. A. Wray, “Fourier-based methods for removing mesh anomalies from angle resolved photoemission spectra,” *Journal of Electron Spectroscopy and Related Phenomena* **260**, 147255 (2022).
 - ³¹Y. Yokoyama, K. Yamagami, Y. Sumiya, H. Shouno, and M. Mizumaki, “Deep prior-based denoising for state-of-the-art scientific imaging and metrology,” Preprint at <https://arxiv.org/abs/2510.09410>.
 - ³²Y. Senba, H. Ohashi, Y. Kotani, T. Nakamura, T. Muro, T. Ohkochi, N. Tsuji, H. Kishimoto, T. Miura, M. Tanaka, *et al.*, “Upgrade of beam-line BL25SU for soft x-ray imaging and spectroscopy of solid using nano- and micro-focused beams at SPring-8,” *AIP Conference Proceedings* **1741** (2016).
 - ³³T. Muro, Y. Senba, H. Ohashi, T. Ohkochi, T. Matsushita, T. Kinoshita, and S. Shin, “Soft X-ray arpes for three-dimensional crystals in the micrometre region,” *Journal of Synchrotron Radiation* **28**, 1631–1638 (2021).
 - ³⁴Y. Senba, H. Kishimoto, Y. Takeo, H. Yumoto, T. Koyama, H. Mimura, and H. Ohashi, “Stable sub-micrometre high-flux probe for soft X-ray ARPES using a monolithic Wolter mirror,” *Journal of Synchrotron Radiation* **27**, 1103–1107 (2020).
 - ³⁵T. Okane, T. Ohkochi, Y. Takeda, S.-i. Fujimori, A. Yasui, Y. Saitoh, H. Yamagami, A. Fujimori, Y. Matsumoto, M. Sugi, *et al.*, “ $4f$ -Derived Fermi Surfaces of $\text{CeRu}_2(\text{Si}_{1-x}\text{Ge}_x)_2$ near the Quantum Critical Point: Resonant Soft-X-Ray ARPES Study,” *Physical Review Letters* **102**, 216401 (2009).
 - ³⁶T. Okane, I. Kawasaki, A. Yasui, T. Ohkochi, Y. Takeda, S.-i. Fujimori, Y. Saitoh, H. Yamagami, A. Fujimori, Y. Matsumoto, *et al.*, “Resonant angle-resolved photoelectron spectroscopy of substitutional solid solutions of CeRu_2Si_2 ,” *Journal of the Physical Society of Japan* **80**, SA060 (2011).
 - ³⁷V. Strocov, “Intrinsic accuracy in 3-dimensional photoemission band mapping,” *Journal of Electron Spectroscopy and Related Phenomena* **130**, 65–78 (2003).
 - ³⁸V. Strocov, L. Lev, F. Alarab, P. Constantinou, X. Wang, T. Schmitt, T. Stock, L. Nicolaï, J. Očenášek, and J. Minár, “High-energy photoemission final states beyond the free-electron approximation,” *Nature Communications* **14**, 4827 (2023).
 - ³⁹A. F. May, Y. Liu, S. Calder, D. S. Parker, T. Pandey, E. Cakmak, H. Cao, J. Yan, and M. A. McGuire, “Magnetic order and interactions in ferrimagnetic $\text{Mn}_3\text{Si}_2\text{Te}_6$,” *Physical Review B* **95**, 174440 (2017).
 - ⁴⁰Y. Ni, H. Zhao, Y. Zhang, B. Hu, I. Kimchi, and G. Cao, “Colossal magnetoresistance via avoiding fully polarized magnetization in the ferrimagnetic insulator $\text{Mn}_3\text{Si}_2\text{Te}_6$,” *Physical Review B* **103**, L161105 (2021).
 - ⁴¹J. Seo, C. De, H. Ha, J. E. Lee, S. Park, J. Park, Y. Skourski, E. S. Choi, B. Kim, G. Y. Cho, *et al.*, “Colossal angular magnetoresistance in ferrimagnetic nodal-line semiconductors,” *Nature* **599**, 576–581 (2021).
 - ⁴²C. Bigi, L. Qiao, C. Liu, P. Barone, M. C. Hatnean, G.-R. Siemann, B. Achinuq, D. A. Mayoh, G. Vinai, V. Polewczyk, *et al.*, “Covalency, correlations, and interlayer interactions governing the magnetic and electronic structure of $\text{Mn}_3\text{Si}_2\text{Te}_6$,” *Physical Review B* **108**, 054419 (2023).
 - ⁴³F. Hadjarab and J. Erskine, “Image properties of the hemispherical analyzer applied to multichannel energy detection,” *Journal of Electron Spectroscopy and Related Phenomena* **36**, 227–243 (1985).
 - ⁴⁴C. Tusche, Y.-J. Chen, C. M. Schneider, and J. Kirschner, “Imaging properties of hemispherical electrostatic energy analyzers for high resolution momentum microscopy,” *Ultramicroscopy* **206**, 112815 (2019).
 - ⁴⁵K. Horiba, T. Imazono, H. Iwasawa, K. Fujii, J. Miyawaki, Y. Ohtsubo, N. Inami, T. Nakatani, K. Inaba, A. Agui, *et al.*, “Design of nano-ARPES beamline at 3-GeV next-generation synchrotron radiation facility, NanoTerasu,” *Journal of Physics: Conference Series* **2380**, 012034 (2022).
 - ⁴⁶C. E. Matt, D. Sutter, A. Cook, Y. Sassa, M. Månsson, O. Tjernberg, L. Das, M. Horio, D. Destraz, C. Fatuzzo, *et al.*, “Direct observation of orbital hybridisation in a cuprate superconductor,” *Nature Communications* **9**, 972 (2018).
 - ⁴⁷M. Horio, K. Hauser, Y. Sassa, Z. Mingazheva, D. Sutter, K. Kramer, A. Cook, E. Nocerino, O. K. Forslund, O. Tjernberg, *et al.*, “Three-

- dimensional Fermi surface of overdoped La-based cuprates,” *Physical Review Letters* **121**, 077004 (2018).
- ⁴⁸T. Yu, C. E. Matt, F. Bisti, X. Wang, T. Schmitt, J. Chang, H. Eisaki, D. Feng, and V. N. Strocov, “The relevance of ARPES to high- T_c superconductivity in cuprates,” *npj Quantum Materials* **5**, 46 (2020).
- ⁴⁹C. Stamm, T. Kachel, N. Pontius, R. Mitzner, T. Quast, K. Holldack, S. Khan, C. Lupulescu, E. Aziz, M. Wietstruk, *et al.*, “Femtosecond modification of electron localization and transfer of angular momentum in nickel,” *Nature Materials* **6**, 740–743 (2007).
- ⁵⁰S. Yamamoto and I. Matsuda, “Time-resolved photoelectron spectroscopies using synchrotron radiation: past, present, and future,” *Journal of the Physical Society of Japan* **82**, 021003 (2013).
- ⁵¹D. J. Higley, K. Hirsch, G. L. Dakovski, E. Jal, E. Yuan, T. Liu, A. A. Lutman, J. P. MacArthur, E. Arenholz, Z. Chen, *et al.*, “Femtosecond X-ray magnetic circular dichroism absorption spectroscopy at an X-ray free electron laser,” *Review of Scientific Instruments* **87** (2016).
- ⁵²K. Takubo, K. Yamamoto, Y. Hirata, Y. Yokoyama, Y. Kubota, S. Yamamoto, S. Yamamoto, I. Matsuda, S. Shin, T. Seki, *et al.*, “Capturing ultrafast magnetic dynamics by time-resolved soft x-ray magnetic circular dichroism,” *Applied Physics Letters* **110** (2017).
- ⁵³P. M. Kraus, M. Zürch, S. K. Cushing, D. M. Neumark, and S. R. Leone, “The ultrafast X-ray spectroscopic revolution in chemical dynamics,” *Nature Reviews Chemistry* **2**, 82–94 (2018).
- ⁵⁴Y. Yokoyama, K. Kawakami, Y. Hirata, K. Takubo, K. Yamamoto, K. Abe, A. Mitsuda, H. Wada, T. Uozumi, S. Yamamoto, *et al.*, “Photoinduced valence dynamics in $\text{EuNi}_2(\text{Si}_{0.21}\text{Ge}_{0.79})_2$ studied via time-resolved x-ray absorption spectroscopy,” *Physical Review B* **100**, 115123 (2019).
- ⁵⁵A. S. Ismail, Y. Uemura, S. H. Park, S. Kwon, M. Kim, H. Elnaggar, F. Frati, Y. Niwa, H. Wadati, Y. Hirata, *et al.*, “Direct observation of the electronic states of photoexcited hematite with ultrafast 2p3d X-ray absorption spectroscopy and resonant inelastic X-ray scattering,” *Physical Chemistry Chemical Physics* **22**, 2685–2692 (2020).
- ⁵⁶Y. Zhang, T. Katayama, A. Chikamatsu, C. Schuessler-Langeheine, N. Pontius, Y. Hirata, K. Takubo, K. Yamagami, K. Ikeda, K. Yamamoto, *et al.*, “Photo-induced antiferromagnetic-ferromagnetic and spin-state transition in a double-perovskite cobalt oxide thin film,” *Communications Physics* **5**, 50 (2022).
- ⁵⁷K. Yamagami, H. Ueda, U. Staub, Y. Zhang, K. Yamamoto, S. H. Park, S. Kwon, A. Mitsuda, H. Wada, T. Uozumi, *et al.*, “4f electron temperature driven ultrafast electron localization,” *Physical Review Research* **6**, 023099 (2024).
- ⁵⁸M. Puppín, Y. Deng, C. W. Nicholson, J. Feldl, N. Schröter, H. Vita, P. Kirchmann, C. Monney, L. Rettig, M. Wolf, *et al.*, “Time-and angle-resolved photoemission spectroscopy of solids in the extreme ultraviolet at 500 kHz repetition rate,” *Review of Scientific Instruments* **90** (2019).
- ⁵⁹B. Lv, T. Qian, and H. Ding, “Angle-resolved photoemission spectroscopy and its application to topological materials,” *Nature Reviews Physics* **1**, 609–626 (2019).
- ⁶⁰J. Madéo, M. K. Man, C. Sahoo, M. Campbell, V. Pareek, E. L. Wong, A. Al-Mahboob, N. S. Chan, A. Karmakar, B. M. K. Mariserla, *et al.*, “Directly visualizing the momentum-forbidden dark excitons and their dynamics in atomically thin semiconductors,” *Science* **370**, 1199–1204 (2020).
- ⁶¹T. Suzuki, S. Shin, and K. Okazaki, “HHG-laser-based time-and angle-resolved photoemission spectroscopy of quantum materials,” *Journal of Electron Spectroscopy and Related Phenomena* **251**, 147105 (2021).
- ⁶²M. Na, A. K. Mills, and D. J. Jones, “Advancing time-and angle-resolved photoemission spectroscopy: The role of ultrafast laser development,” *Physics Reports* **1036**, 1–47 (2023).